CD9 shapes glucocorticoid sensitivity in pediatric B-cell precursor acute lymphoblastic leukemia

Chi Zhang,[1] Kathy Yuen Yee Chan,[1] Wing Hei Ng,[1] John Tak Kit Cheung,[1] Qiwei Sun,[1] Han Wang,[1] Po Yee Chung,[1] Frankie Wai Tsoi Cheng,[2] Alex Wing Kwan Leung,[1] Xiao-Bing Zhang,[3] Po Yi Lee,[1] Siu Ping Fok,[1] Guanglan Lin,[1] Ellen Ngar Yun Poon,[4] Jian-Hua Feng,[5] Yan-Lai Tang,[6] Xue-Qun Luo,[6] Li-Bin Huang,[6] Wei Kang,[7] Patrick Ming Kuen Tang,[7] Junbin Huang,[8] Chun Chen,[8] Junchao Dong,[9] Ester Mejstrikova,[10] Jiaoyang Cai,[11] Yu Liu,[11] Shuhong Shen,[11] Jun J Yang,[12] Patrick Man Pan Yuen,[1] Chi Kong Li[1,13] and Kam Tong Leung[1,13]

[1]Department of Paediatrics, The Chinese University of Hong Kong, Shatin, Hong Kong; [2]Department of Paediatrics and Adolescent Medicine, Hong Kong Children's Hospital, Kowloon Bay, Hong Kong; [3]Haihe Laboratory of Cell Ecosystem, Institute of Hematology & Blood Diseases Hospital, Tianjin, China; [4]School of Biomedical Sciences, The Chinese University of Hong Kong, Shatin, Hong Kong; [5]Department of Hematology, The First Affiliated Hospital of Wenzhou Medical University, Wenzhou, China; [6]Department of Pediatrics, The First Affiliated Hospital, Sun Yat-sen University, Guangzhou, China; [7]Department of Anatomical and Cellular Pathology, The Chinese University of Hong Kong, Shatin, Hong Kong; [8]Division of Hematology/Oncology, Department of Pediatrics, The Seventh Affiliated Hospital, Sun Yat-sen University, Shenzhen, China; [9]Department of Immunology, Zhongshan School of Medicine, Sun Yat-sen University, Guangzhou, China; [10]CLIP-Department of Pediatric Hematology and Oncology, Second Faculty of Medicine, Charles University and University Hospital Motol, Prague, Czech Republic; [11]Department of Hematology/Oncology, Shanghai Children's Medical Center, School of Medicine, Shanghai Jiao Tong University, Shanghai, China; [12]Department of Pharmaceutical Sciences, St. Jude Children's Research Hospital, Memphis, TN, USA and [13]Hong Kong Hub of Paediatric Excellence, The Chinese University of Hong Kong, Shatin, Hong Kong

Correspondence: K.T. Leung
ktleung@cuhk.edu.hk

Received: February 15, 2023.
Accepted: March 22, 2024.
Early view: April 4, 2024.

https://doi.org/10.3324/haematol.2023.282952

Supplemental Information for Zhang et al

"CD9 shapes glucocorticoid sensitivity in pediatric B-cell precursor acute lymphoblastic leukemia"

Supplemental Methods

Cells and CD9 characterization

BCP-ALL cell lines 697, BV-173, KOPN-8, RS4;11 and SEM (DSMZ, Braunchweig, Germany) as well as SUP-B15 (ATCC, Manassas, VA, USA) were maintained in RPMI-1640 medium (Life Technologies, Waltham, MA, USA) supplemented with 10% fetal bovine serum (Life Technologies). The cell surface CD9 expression was characterized by CD9-PE antibody (clone M-L13; BD Biosciences, San Jose, CA, USA). Primary lymphoblasts were recovered from cryopreserved, diagnostic bone marrow samples of pediatric BCP-ALL patients by density gradient centrifugation using Ficoll-Paque Plus (GE Healthcare, Chicago, IL, USA) and delineated for purity with fluorochrome-conjugated antibodies: CD9-PE, CD19-BV605 (clone HIB19; BD Biosciences), CD34-PE-Cy7 (clone 8G12; BD Biosciences), and CD45-APC (clone J.33; Beckman Coulter, Brea, CA, USA). Cell surface CD9 expression on $CD45^{dim/-}CD34^{+/-}CD19^{+}$ blasts was determined by flow cytometry (LSRFortessa, BD Biosciences), with negative populations defined by respective isotype controls. All FACS data were analyzed using FlowJo software v10.4 (TreeStar, Ashland, OR, USA).

Drug sensitivity assay

BCP-ALL cell lines (5×10^4-1×10^5) were seeded into 96-well plates (Corning, NY, USA) and treated with DMSO control or 0.1 nM-100 μM of Pred, Dex, Ara-C, DNR, VCR, or MTX (Selleckchem, Houston, TX, USA) for 72 hours. In some experiments, leukemic cells were treated with Pred or Dex in combination with 0.1-100 μM of trametinib (MedChemExpress, Monmouth Junction, NJ, USA). Cell proliferation was measured using the CellTiter MTS solution according to the manufacturer's instructions (Promega, Madison, WI, USA).

Primary lymphoblasts (1.6×10^5) were seeded onto GFP-expressing, hTERT-immortalized mesenchymal stem cells (MSCs, 1×10^4) and treated with DMSO or 0.1 nM-100 μM of Pred or Dex for 96 hours.[1] On some occasions, lymphoblasts were concomitantly treated with trametinib and/or ruxolitinib (MedChemExpress) at the indicated concentrations. Cells were recovered by 0.25% trypsin (Gibco, Grand Island, NY, USA). Leukemic cells were identified with CD19-BV421 (clone HIB19; BD Biosciences). Annexin V^-/$7\text{-}AAD^-$ viable cells were recognized using the Apoptosis Detection Kit (BD Biosciences) by flow cytometry. The percentage of viable cells was normalized against DMSO

controls with outliers removed before curve fitting. The half-maximal inhibitory concentrations (IC50s) were calculated from the dose-response curves by nonlinear regression using the GraphPad Prism software (GraphPad, San Diego, CA, USA). The IC50 values were designated as the highest dose (*i.e.* 100 μM) whenever the cell viability remained >50% across the entire dose range.[2] Hierarchical clustering was performed using the Euclidean distance metric and Ward's minimum variance method for linkage[3] to generate drug clusters (clusters A and B) with the Pheatmap package in R v3.4.1 (http://cran.r-project.org/web/packages/pheatmap/index.html). The Bliss score indicating synergy of drug combinations was calculated using SynergyFinder.[4]

Patient cohort

Children with BCP-ALL were recruited from three clinical studies conducted in the Prince of Wales Hospital, Hong Kong between 1997 and 2015: HKALL 97,[5] IC-BFM ALL 2002[6] and CCLG 2008.[7] These clinical studies commonly adopted a Berlin-Frankfurt-Münster (BFM)-based treatment protocol, with a prephase of 7-day oral Pred at 60 mg/m^2 before the commencement of multiagent chemotherapy. Baseline demographic data, clinical parameters and pathologic variables of the recruited patients were retrieved from the medical records. Specimens were collected with informed written consent following the Declaration of Helsinki. The study was approved by the Joint Chinese University of Hong Kong – New Territories East Cluster Clinical Research Ethics Committee.

Lentiviral vectors and transduction

For gain-of-function studies, the human CD9 full-length open reading frame (Open Biosystems, Huntsville, AL, USA) was inserted into the pRSC-SFFV-E2A-GFP-Wpre lentiviral backbone by PCR cloning and verified by Sanger sequencing (ABI 3130 Genetic Analyzer, Applied Biosystem, Foster City, CA, USA). For loss-of-function studies, a single-guide RNA (sgRNA) targeting human CD9 (GGGATATTCCCACAAGGATG) or a non-targeting sgRNA (GCACTCACATCGCTACATCA) was inserted into the pRSC-U6-SFFV-Cas9-E2A-GFP-Wpre lentiviral backbone. VSVG-pseudotyped vectors were packaged in 293T cells (ATCC), with functional viral titers determined by transduction of HT1080 cells (ATCC) followed by flow cytometry analysis.[8] CD9^{low} cells were transduced with control GFP-only or CD9-GFP lentiviral particles, whereas CD9^{high} cells were transduced with control sgRNA-GFP or CD9 sgRNA-GFP lentiviral particles at a multiplicity of infection of 4-8 for 48 hours

in non-TC-treated plates precoated with RetroNectin (50 μg/mL; Takara Bio Inc., Shiga, Japan). The transduction efficiency was determined by quantification of GFP^+ cells coupled with CD9-APC antibody staining (clone M-L13; BD Biosciences). Stable cell lines were generated by selection with puromycin (1 μg/mL; Life Technologies) or cell sorting (FACSAria Fusion, BD Biosciences).

Western blotting and co-immunoprecipitation

BCP-ALL cells (5×10^6), with or without GC treatments, were lysed in RIPA buffer (Sigma-Aldrich, St. Louis, MO, USA) supplemented with protease inhibitor cocktails (Roche Diagnostics, Indianapolis, IN, USA) to obtain total cell lysates. On some occasions, subcellular components were recovered with a Cell Fractionation Kit following the manufacturer's protocols (Cell Signaling Technology, Danvers, MA, USA). Protein concentrations were measured with the DC Protein Assay Kit (Bio-Rad, Hercules, CA, USA). Lysates (30-50 μg) were separated by SDS-PAGE and probed with antibodies against CD9 (clone D8O1A), phospho-NR3C1 (Ser211, polyclonal), phospho-NR3C1 (Ser226, clone D9D3V), NR3C1 (clone D6H2L), phospho-MEK1/2 (Ser217/221, clone 41G9), MEK1/2 (clone 47E6), phospho-ERK1/2 (Thr202/Tyr204, clone D13.14.4E) or ERK1/2 (clone 137F5), with GAPDH (clone 14C10) or histone H3 (clone D1H2) as loading controls where appropriate. All primary antibodies were from Cell Signaling Technology and used at a fixed dilution of 1:1000. The reactions were developed with peroxidase-conjugated goat-anti-rabbit secondary antibodies (1:5000) followed by detection with SignalFire Plus ECL Reagent or SiganlFire Elite ECL Reagent (Cell Signaling Technology). Chemiluminescence snapshots were captured on the Alliance Q9 Advanced Imager (UVItec, Cambridge, UK).

For co-immunoprecipitation assays, BCP-ALL cells (9×10^8) treated with GCs were lysed in 1% Brij97 buffer (Sigma-Aldrich). Cell lysates (900 μg) were immunoprecipitated with 10 μg isotype control IgG_{2b} (clone 20016; R&D Systems, Minneapolis, MN, USA) or CD9 antibody (clone MM2/57; Millipore, Billerica, MA, USA) at 4°C overnight. Immune complexes were captured with protein A/G agarose (Pierce, Waltham, MA, USA) and separated by SDS-PAGE. Immunoblots were then probed with antibodies against CD9 (clone D8O1A, Cell Signaling Technology), NR3C1 (clone D6H2L, Cell Signaling Technology), CD81 (clone D3N2D, Cell Signaling Technology) or EWI-2 (clone: 2587A, R&D systems), as described.

RNA sequencing

Total RNA was extracted from patient samples or Dex-treated BCP-ALL cells using TRIzol reagent (Life Technologies) and RNeasy Micro Kit (Qiagen, Hilden, Germany). After ribosomal RNA removal (Ribo-zero, Epicenter, Madison, WI, USA), cDNA libraries were generated by the NEBNext Ultra Directional RNA Library Prep Kit (New England BioLabs, Ipswich, MA, USA) and sequenced on a NovaSeq 6000 platform (Illumina, San Diego, CA, USA) to yield 10 Gb raw data. Adapter contamination and low-quality reads were filtered, resulting in clean reads ranging from 63M to 73M. Alignment of reads to the human reference genome (hg38) was performed using STAR-2.7.8a.[9] Gene assignments were based on Ensembl 104 build gene models. Counts per million mapped reads (CPM) were generated with Partek Flow software v10.0 (Partek, St. Louis, MO, USA). Gene-specific analysis (GSA) was applied to generate differentially expressed genes (DEGs) using cutoffs of ≥1.5-fold change and FDR<0.05. To curate *NR3C1* isoform expression[10] and hotspot mutations[11] from RNA-seq data, transcript per kilobase million (TPM) normalization and variant calling were respectively performed with Partek Flow.

Quantitative RT-PCR

First-strand cDNA was generated from 500 ng of purified RNA using the High-Capacity cDNA Reverse Transcription Kit (Life Technologies). Quantitative PCRs were set up by mixing 10 ng of cDNA template with TaqMan Gene Expression Master Mix (Life Technologies) and TaqMan assays (Life Technologies). Reactions (50°C, 2 min; 95°C, 10 min; 45 cycles of 95°C, 15 s and 60°C, 1 min) were performed on the QuantStudio 5 Real-Time PCR system (Applied Biosystem). The expression of GC-responsive genes was analyzed by the comparative C_T method and normalized to the expression of *GAPDH*.

Chromatin immunoprecipitation sequencing

Chromatin immunoprecipitation (ChIP) was performed using the SimpleChIP Enzymatic Chromatin IP Kit following the manufacturer's protocols (Cell Signaling Technology). Briefly, Dex-treated BCP-ALL cells were crosslinked with 37% formaldehyde (Sigma-Aldrich) for 10 minutes and quenched with glycine for 5 minutes. Chromatin was isolated from the cell pellets and sonicated to generate 150-900 bp DNA fragments as monitored by agarose gel electrophoresis. Processed chromatin (40 μg) was

immunoprecipitated with control IgG or NR3C1 antibody (clone D8H2, Cell Signaling Technology) at 4ºC overnight. DNA was purified from the eluted chromatin, and NGS was performed with the NovoSeq 6000 platform (Illumina) to produce an average of 30 million reads per sample. High quality sequences were mapped to the hg38 reference genome using BWA.[12] Fragment estimation, identification of local noise parameters and peak calling on the aligned reads was performed with MACS3.[13] Peaks indicative of NR3C1 binding were curated and annotated using ChIPseeker.[14,15] Input DNA was used as the background control.

Xenograft experiments

Animal experiments were conducted in accordance with procedures approved by the Institutional Animal Experimentation Ethics Committee. Female NOD.Cg-*Prkdc*^{scid}*Il2rg*^{tm1Wjl}/SzJ (NSG) mice (8-10-week-old; Jackson Laboratory, Bar Harbor, ME, USA) were infused with luciferase-expressing BCP-ALL cells (1×10^6 cells/mouse) *via* tail veins. On day 3 post-infusion, animals were randomized to receive daily administration of vehicle solutions (PBS by intraperitoneal injection and corn oil by oral gavage), Dex (5 mg/kg in PBS by intraperitoneal injection), trametinib (5 mg/kg in corn oil by oral gavage) or their combination.[16] The treatment was performed on a 5 days on and 2 days off schedule for a duration of 2 weeks. When humane endpoints were reached (≥20% weight loss, obvious distress or hindleg paralysis), the systemic leukemic load was evaluated using the IVIS 200 In Vivo Imaging System (Xenogen, Alameda, CA, USA) following the application of D-Luciferin (150 mg/kg; Promega, Madison, WI, USA) and anaesthetization with 2.5% isoflurane (Zowtis, Parippany, NJ, USA). Luminescence signals were captured using the Living Image software (Xenogen). To determine the medullary leukemic burden, single cell suspensions were prepared from the femurs of euthanized animals. After red cell lysis and Fc receptor blocking, leukemic cells were measured by staining with human-specific antibodies against CD19-PE (clone HIB19) and CD45-APC (clone J.33) followed by flow cytometry analyses.

Statistical analyses

The statistical methods applied for individual experiments are indicated in the table footnotes or figure legends. Analyses were performed with GraphPad Prism v8.3.0 (GraphPad) or SPSS v26.0 (IBM Corp, Armonk, NY, USA). *P* values of <0.05 were considered statistically significant.

Supplemental Table 1. Taqman assays

Gene name	Gene symbol	Probe ID
BCL2 like 11	*BCL2L11*	Hs01076940_m1
CD9	*CD9*	Hs00233521_m1
Glyceraldehyde-3-phosphate dehydrogenase	*GAPDH*	Hs99999905_m1
Nuclear receptor subfamily 3 group C member 1	*NR3C1*	Hs00353740_m1
Signal transducer and activator of transcription 5A	*STAT5A*	Hs00559643_m1
TSC22 domain family member 3	*TSC22D3*	Hs00608272_m1
Zinc finger and BTB domain containing 16	*ZBTB16*	Hs00232313_m1

Supplemental Table 2. Characteristics of BCP-ALL samples undergone *ex vivo* drug testing

Sample Code	$CD9^+$ blasts (%)	CD9 group	Gender	Age at diagnosis (years)	Diagnostic WBC ($x10^9$/L)	Response to Pred prephase	Dex IC50 (nM)	Pred IC50 (nM)	Cytogenetics	Gene fusion
Pt_82	0.3	-	M	4.6	5.3	Good	34.1	452	46,XY[24]	*ETV6-RUNX1*
Pt_91	5.2	-	F	2.4	7.0	Poor	>100000	>100000	30,XX,-1,-2,-3,-4,-5,-6,-7,-9,-12,-13,-15,-16,-17,-19,-20,-22[4]/46,XX[20]	NIL
Pt_138	23.9	+	M	11.3	21.3	Good	9.4	172	46,XY,t(12;17)(p13;q21)[9]/47,idem,+del(8)(p21)(4)/47,idem,+1,der(1;15)(q10;q10),+del(8)(p21)[4]/46,XY[6]	NIL
Pt_187	2.2	-	F	9.6	5.4	Good	37.7	326	46,XX[20]	NIL
Pt_238	9.3	-	M	4.1	208.6	Good	5469	15919	46,XY,t(9;22)(q34;q11.20[1]	*BCR-ABL1*
Pt_338	100	+	F	6.3	10.7	N/A	6.8	65.8	46,XX,del(4)(q21q25),del(9)(p22),der(9;12(q10;q10),+mar[17]	NIL
Pt_371	99.9	+	F	3.1	434.6	N/A	30.5	16.6	45,XX,t(9;22)(q34;q11.2),-18[8]/46,XY[2]	*BCR-ABL1*
Pt_372	3.5	-	F	1.2	148.7	N/A	>100000	>100000	46,XX,t(4;11)(q21;q23)[3]/48,idem,+X,+1,-13,i(17)(q10,der(20)t(13;20)(q12;q13.3),+21[5]/46,XX[1]	*KMT2A-AFF1*
Pt_379	100	+	M	12.0	112.0	N/A	59.4	365	47,XY,+X,-6,-9,+mar[17]/46,XY[3]	NIL
Pt_402	88.6	+	M	8.5	12.4	N/A	1119	8445	46,XY,der(1)t(1;1*)(p36.3;q21),t(1;19)(q23;p13.3)[12]/46,XY,t(1;19)(q23;p13.3),-9,+mar[4]/46,XY[4]	*TCF3-PBX1*
Pt_424	97.8	+	M	5.5	72.6	N/A	9.5	90.3	46,XY[20]	NIL
Pt_436	67.7	+	M	6.0	67.0	N/A	104	5874	46,XY,del(4)(q12q12)[5]/46,XY[20]	NIL
Pt_440	38.7	+	M	8.8	3.2	N/A	9.3	83.8	47,XY,del(6)(q21q25),del(11)(q13q23),-12,+16,+mar[8]/47,XY,del(6)(q21q25),add(11)(q23),-12,+16, +mar[6]/46,XY[2]	*ETV6-RUNX1*
Pt_448	99.8	+	M	14.1	87.4	N/A	149	2331	46,XY,del(16)(q12.1)[23]/46,XY[6]	NIL
Pt_453	99.5	+	M	5.8	25.7	N/A	2.4	22.4	46,XY,-18,der(19)t(1;19)(q23;p13.3),+mar[11]/46,idem,add(12)(p11.2)/46,XY[5]	*TCF3-PBX1*
Pt_456	99.5	+	M	5.2	21.1	N/A	3799	17655	53~54,XY,+X[11],+6[11],+10[10],-12[11],+14[11],+14[10],+17[6],+18[10],add(19)(q13.3)[11],+21[11], +21[4],+mar[11][cp11]/46,XY[14]	NIL
Pt_464	98.8	+	F	5.2	3.5	N/A	32.4	518	60<3n>,XX,-X,-1,-2,-4,-9,-11,-12,-13,+14,-15,-16,add(16)(p13.3),-19,-20,+21,+mar[6]/60<3n>,idem, add(11)(q13)[2]/46,XX[9]	NIL
Pt_465	9.4	-	F	8.8	1.2	N/A	53.6	334	46,XX[16]	*ETV6-RUNX1*

Supplemental Table 3. Association of CD9 with clinical characteristics of BCP-ALL patients

Clinical Parameters	All patients (n = 182)		$CD9^+$ patients (n = 146)		$CD9^-$ patients (n = 36)		$CD9^+$ *vs* $CD9^-$
	No.	**%**	**No.**	**%**	**No.**	**%**	***P***
Age, years							
Median (IQR)	4.4 (2.7-7.9)		4.3 (2.6-7.8)		4.8 (2.7-8.0)		0.718
<1	16	8.8	14	9.6	2	5.5	0.742
1 - <10	134	73.6	105	71.9	29	80.6	0.292
≥10	32	17.6	27	18.5	5	13.9	0.516
Sex							
Male	113	62.1	90	61.6	23	63.9	0.804
Female	69	37.9	56	38.4	13	36.1	
WBC, $\times 10^9$/L							
Median (IQR)	13.4 (6.3-54.8)		13.4 (6.3-54.8)		14.2 (6.2-51.3)		0.967
<50	134	73.6	107	73.3	27	75.0	0.835
≥50	48	26.4	39	26.7	9	25.0	
Cytogenetics							
Hyperdiploidy	30	16.5	30	20.5	0	0	***<0.001***
BCR-ABL1	11	6.0	8	5.5	3	8.3	0.457
ETV6-RUNX1	35	19.2	18	12.3	17	47.3	***<0.001***
KMT2A-rearranged	14	7.7	11	7.5	3	8.3	1.000
TCF3-PBX1	10	5.5	10	6.9	0	0	0.215
Others	82	45.1	69	47.3	13	36.1	0.229

Abbreviations: IQR, interquartile range; WBC, white blood cells.
Statistics: continuous variables, Mann-Whitney U test; categorical data, Pearson's Chi-square test or Fisher's exact test.

Supplemental Table 4. Univariate and multivariate analyses of prednisone response

	Univariate			Multivariate		
Variables	**OR**	**95% CI**	***P***	**OR**	**95% CI**	***P***
CD9*						
Positive	1					
Negative	3.7	1.3-10.7	***0.017***	5.1	1.5-17.3	***0.009***
WBC* (× 10^9/L)						
<50	1					
≥50	10.8	3.3-35.6	***<0.001***	13.1	3.7-46.0	***<0.001***
Age (years)						
1-9.9	1					
<1	3.2	0.8-13.3	0.109			
≥10	2.0	0.6-6.9	0.282			
Sex						
Female	1					
Male	1.4	0.5-4.2	0.567			
Hyperdiploidy						
Present	1					
Absent	0.3	0.1-2.5	0.272			
BCR-ABL1*						
Absent	1					
Present	7.6	1.9-29.5	***0.004***	3.4	0.7-17.7	0.145
***KMT2A*-rearrangement**						
Absent	1					
Present	1.8	0.4-9.0	0.456			
TCF3-PBX1						
Absent	1					
Present	1.2	0.1-9.8	0.890			
B-others						
Absent	1					
Present	1.2	0.4-3.5	0.678			

Abbreviations: OR, odds ratio; CI, confidence interval.
Statistics: Multivariate analysis: binary logistic regression model with backward likelihood method.
*Variables included in multivariate analysis.
ETV6-RUNX1 is not included in the analyses because none of the patients were poor prednisone responders.

Supplemental Table 5. Isoform expression and mutational status of *NR3C1* in BCP-ALL cells

Cell type	CD9 group	Dex IC50 (nM)	Pred IC50 (nM)	*NR3C1* Isoform (TPM)			*NR3C1* mutation	
				GRα	GRβ	GRγ	p. Y478C	p. R477H
BCP-ALL cell line								
SEM	low	530	27009	18.7	0	2.3	WT	WT
KOPN-8	low	855	11705	17.2	0	0.8	WT	WT
RS4;11	high	1.1	15.5	73.8	0	5.8	WT	WT
697	high	25.9	421	7.7	0	0.6	WT	WT
SUP-B15	high	3.6	46.7	24.7	0.3	2.4	WT	WT
BV-173	high	5.5	77.6	111	12.3	20.6	WT	WT
Patient sample*								
Pt_82	-	34.1	452	6.1	0	1.8	WT	WT
Pt_91	-	>100000	>100000	9.5	0	2.0	WT	WT
Pt_138	+	9.4	172	18.3	0	4.0	WT	WT
Pt_187	-	37.7	326	12.5	0	1.9	WT	WT
Pt_238	-	5469	15919	15.1	1.3	0.7	WT	WT
Pt_338	+	6.8	65.8	11.9	0	0.9	WT	WT
Pt_371	+	30.5	16.6	17.2	0	2.4	WT	WT
Pt_372	-	>100000	>100000	8.6	0	2.7	WT	WT
Pt_379	+	59.4	365	10.9	3.4	1.3	WT	WT
Pt_402	+	1119	8445	9.7	0	2.4	WT	WT
Pt_424	+	9.5	90.3	9.7	0	2.4	WT	WT
Pt_436	+	104	5874	12.1	0.3	2.4	WT	WT
Pt_440	+	9.3	83.8	40.6	0	7.9	WT	WT
Pt_448	+	149	2331	19.3	0	3.7	WT	WT
Pt_453	+	2.4	22.4	12	0	1.0	WT	WT
Pt_456	+	3799	17655	22.2	0	3.5	WT	WT
Pt_464	+	32.4	518	18.6	0	3.5	WT	WT
Pt_465	-	53.6	334	12.1	0.1	4.2	WT	WT

Abbreviations: TPM, transcripts per kilobase million; WT, wild type.
*****$NR3C1$ isoform expression ($CD9^+$ *vs.* $CD9^-$): GRα, P=0.109; GRβ, P=0.868; GRγ, P=0.406.
Statistics: two-tailed, unpaired Student's *t*-test.

Supplemental Table 6. List of differential expressed genes in Dex-treated SEM cells

Gene symbol	FDR step up (CD9-Dexa vs. CD9-DMSO)	Fold change (CD9-Dexa vs. CD9-DMSO)	FDR step up (GFP-Dexa vs. GFP-DMSO)	Fold change (GFP-Dexa vs. GFP-DMSO)	Gene list	Selected gene ontology*	Reported GC responsive genes
SMIM3	3.75E-06	18.518	1.09E-05	16.575	CD9 & GFP		
NDRG2	1.52E-04	10.111	5.81E-03	8.170	CD9 & GFP		Mir *et al*, 2019[17]
ISG20	1.23E-09	7.954	4.84E-09	7.832	CD9 & GFP		Tissing *et al*, 2007[18]
GSDME	7.30E-04	7.558	3.74E-03	6.143	CD9 & GFP		Webb *et al,* 2007[19]
LCN10	6.28E-03	7.532	5.16E-02	6.723	CD9		
EPS8	4.11E-11	6.714	8.65E-10	6.209	CD9 & GFP		
MYRIP	2.62E-11	6.659	2.75E-10	6.147	CD9 & GFP		
FKBP5	1.68E-140	6.035	5.18E-126	5.699	CD9 & GFP		Nold *et al,* 2021[20]
TSC22D3	9.16E-31	5.909	1.40E-24	5.437	CD9 & GFP		Tissing *et al*, 2007[18]
GSN	2.81E-11	5.732	3.21E-11	5.423	CD9 & GFP	Programmed cell death	
SCML4	1.11E-04	5.514	2.36E-04	5.810	CD9 & GFP		
DDIT4	2.04E-43	5.492	1.15E-39	5.317	CD9 & GFP		Wolff *et al*, 2014[21]
LDLRAD4	7.46E-08	5.383	1.18E-06	4.431	CD9 & GFP		
MTUS1	3.42E-07	5.217	5.67E-05	4.121	CD9 & GFP		
XACT	2.11E-04	4.569	1.08E-02	3.172	CD9 & GFP		
GUCY1A2	7.30E-04	4.459	1.21E-01	2.722	CD9		
ADPRHL1	7.60E-03	4.206	1.98E-02	3.716	CD9 & GFP		
FZD4	6.17E-03	3.533	1.16E-01	2.896	CD9		Shi *et al*, 2015[22]
AMOT	2.51E-13	3.411	5.37E-12	3.203	CD9 & GFP		
LONRF1	3.96E-18	3.396	4.33E-12	2.844	CD9 & GFP		
NT5DC2	2.68E-16	3.353	1.43E-11	2.813	CD9 & GFP		
SLC44A1	1.12E-45	3.353	1.23E-39	3.329	CD9 & GFP		
MYO10	8.56E-09	3.228	1.47E-08	3.046	CD9 & GFP		
ZHX3	1.80E-06	3.148	1.69E-06	3.168	CD9 & GFP		
KLF9	3.79E-06	3.037	1.11E-04	2.831	CD9 & GFP		Tissing *et al*, 2007[18]
CRMP1	5.22E-03	2.939	5.60E-03	2.537	CD9 & GFP		
BTNL9	8.52E-03	2.924	1.08E-02	2.933	CD9 & GFP		
RECK	2.19E-03	2.863	1.08E-02	2.713	CD9 & GFP		
ZBTB16	4.85E-02	2.856	3.97E-02	1.980	CD9 & GFP		Tissing *et al*, 2007[18]
AC104530.1	2.77E-04	2.808	1.49E-01	1.962	CD9		
PAG1	1.57E-02	2.775	5.66E-01	1.941	CD9		
CXCR4	4.18E-11	2.745	3.04E-11	2.816	CD9 & GFP		Hong *et al*, 2020[23]
SMAP2	6.85E-08	2.740	2.60E-08	2.938	CD9 & GFP		
IL6ST	5.18E-07	2.708	2.70E-07	2.683	CD9 & GFP		
FGFR1	1.97E-06	2.705	1.18E-06	2.716	CD9 & GFP		Choi *et al*, 2022[24]
DAAM1	2.86E-04	2.700	5.75E-03	2.137	CD9 & GFP		

CLN8	1.52E-04	2.602	4.56E-04	2.866	CD9 & GFP		
HUNK	5.96E-03	2.600	2.74E-03	2.868	CD9 & GFP		
FZD8	8.90E-04	2.569	1.13E-02	2.256	CD9 & GFP		
NFIL3	2.97E-02	2.558	1.55E-01	2.438	CD9		Tissing *et al*, 2007[18]
ANKRD33B	6.17E-09	2.506	9.39E-09	2.526	CD9 & GFP		
MAP3K5	2.47E-06	2.403	3.74E-04	2.092	CD9 & GFP	Programmed cell death	Chen *et al*, 2023[25]
SLC27A3	2.15E-02	2.396	9.83E-02	2.180	CD9		
RASA2	4.48E-03	2.352	5.14E-03	2.382	CD9 & GFP		
NFKBIA	4.79E-03	2.322	3.93E-03	2.321	CD9 & GFP		Zhang *et al*, 2023[26]
CRISPLD1	9.04E-03	2.319	1.37E-02	2.483	CD9 & GFP		
SPRY4	4.96E-02	2.302	3.67E-01	1.847	CD9		
GAB1	8.40E-12	2.297	3.69E-09	2.153	CD9 & GFP		Sharma *et al*, 2015[27]
PER1	6.64E-03	2.258	2.44E-03	2.327	CD9 & GFP	Regulation of glucocorticoid receptor signaling pathway	Yurtsever *et al*, 2019[28]
MGAT4A	5.70E-04	2.240	1.07E-02	1.929	CD9 & GFP		
ZFP36L2	3.78E-12	2.229	9.37E-14	2.429	CD9 & GFP		Tissing *et al*, 2007[18]
CD109	3.96E-17	2.220	3.95E-12	1.962	CD9 & GFP		
USP12	3.78E-09	2.172	5.25E-04	1.702	CD9 & GFP		
IRAK3	1.12E-13	2.152	3.39E-08	1.881	CD9 & GFP		
TMEM65	3.61E-10	2.146	2.95E-07	1.961	CD9 & GFP		
SYNE3	5.45E-10	2.080	2.75E-10	2.136	CD9 & GFP		
INSR	6.62E-20	2.063	4.35E-15	1.905	CD9 & GFP		Tissing *et al*, 2007[18]
KLF7	7.30E-04	2.035	1.90E-03	2.026	CD9 & GFP		
CLNS1A	7.30E-04	1.976	8.39E-02	1.612	CD9		
TGFBR2	3.79E-06	1.928	3.74E-03	1.627	CD9 & GFP		Wang *et al*, 2022[29]
SMARCA2	1.58E-15	1.890	9.78E-12	1.794	CD9 & GFP		
CLMN	7.60E-03	1.881	4.27E-02	1.717	CD9 & GFP		
SYNJ2	1.30E-03	1.877	1.05E-02	1.713	CD9 & GFP		
TACC1	1.17E-06	1.861	2.38E-04	1.661	CD9 & GFP		
SLC44A2	2.39E-06	1.842	1.83E-06	1.827	CD9 & GFP		
BTG1	7.95E-05	1.841	8.47E-03	1.628	CD9 & GFP		Scheijen *et al*, 2017[30]
YBX3	2.84E-06	1.839	2.26E-05	1.791	CD9 & GFP		
BCL2L11	3.79E-06	1.839	4.61E-03	1.584	CD9 & GFP	Programmed cell death	Saenz *et al*, 2015[31]
CTSB	7.30E-04	1.833	5.17E-02	1.624	CD9		
SORT1	7.95E-05	1.829	3.06E-03	1.689	CD9 & GFP		
RASAL2	1.93E-02	1.815	1.29E-01	1.719	CD9		
CD53	1.98E-03	1.808	3.84E-02	1.617	CD9 & GFP		
FOSL2	5.05E-06	1.800	2.57E-06	1.819	CD9 & GFP	Programmed	

						cell death	
REEP3	4.89E-09	1.797	1.42E-04	1.574	CD9 & GFP		
GLUL	7.47E-17	1.788	4.38E-15	1.748	CD9 & GFP		
MAP2K1	3.12E-02	1.781	7.98E-02	1.704	CD9	Response to glucocorticoid	Tissing *et al*, 2007[18]
NISCH	1.02E-04	1.781	2.16E-04	1.802	CD9 & GFP		
WWC3	1.62E-02	1.759	9.58E-02	1.646	CD9		
SNX30	8.40E-12	1.754	3.10E-08	1.618	CD9 & GFP		
MAP3K1	1.41E-06	1.751	2.60E-08	1.903	CD9 & GFP		
KLF13	1.74E-08	1.726	7.08E-06	1.593	CD9 & GFP		Cruz-Topete *et al*, 2016[32]
CD96	7.30E-04	1.714	5.17E-02	1.508	CD9		
NUDT4	1.31E-05	1.701	1.10E-05	1.741	CD9 & GFP		
DOCK7	2.26E-02	1.701	3.00E-01	1.557	CD9		
CSPG4	2.48E-02	1.679	1.90E-03	1.865	CD9 & GFP		
MEF2A	4.30E-06	1.646	1.11E-04	1.572	CD9 & GFP		
OGFRL1	5.54E-03	1.622	2.48E-01	1.427	CD9		Jiang *et al*, 2020[33]
TRAK2	3.98E-02	1.618	1.16E-01	1.574	CD9		
AGO4	2.22E-03	1.603	3.07E-01	1.387	CD9		
LRRFIP1	1.80E-05	1.583	9.19E-05	1.540	CD9 & GFP		
ANAPC16	4.71E-02	1.570	1.34E-01	1.541	CD9		
EZR	1.53E-05	1.537	1.04E-04	1.471	CD9		Tissing *et al*, 2007[18]
TPD52	2.59E-03	1.530	8.91E-03	1.505	CD9 & GFP		
AKAP13	3.48E-03	1.506	6.20E-02	1.406	CD9	Regulation of glucocorticoid receptor signaling pathway	Koide *et al*, 2015[34]
CORO1C	9.15E-03	1.504	4.40E-02	1.431	CD9		
PTK2B	4.43E-05	1.504	4.97E-03	1.400	CD9		
PDE7A	2.69E-02	1.503	3.06E-01	1.422	CD9		Dong *et al*, 2010[35]
RPL41	1.05E-02	-1.501	1.00E+00	-1.005	CD9		
MYO18A	9.86E-03	-1.512	1.13E-02	-1.497	CD9		
H2BC18	5.55E-04	-1.584	1.00E+00	-1.213	CD9		
H4C12	3.98E-02	-1.603	1.00E+00	-1.174	CD9		
FTL	3.40E-03	-1.642	4.68E-01	-1.318	CD9		
CLEC11A	2.05E-03	-1.693	1.24E-01	-1.463	CD9		
RPS11	2.02E-04	-1.708	1.00E+00	-1.095	CD9		
BMF	1.73E-02	-1.766	8.31E-02	-1.667	CD9	Programmed cell death	Chen *et al*, 2010[36]
SASH3	1.90E-02	-1.843	1.39E-01	-1.636	CD9		
TMSB10	2.05E-03	-1.880	9.58E-01	-1.336	CD9		
H2AC7	4.19E-03	-2.830	1.00E+00	-1.114	CD9		

NRP1	1.38E-01	5.834	7.94E-03	6.409	GFP
SPRY1	5.97E-02	4.404	3.84E-02	4.989	GFP
SNX9	5.74E-02	4.808	2.96E-02	4.547	GFP
PLCG1	5.18E-02	2.728	4.77E-03	3.701	GFP
ITGA9	1.28E-01	2.724	2.27E-02	3.442	GFP
LAPTM5	1.83E-06	1.485	1.42E-10	1.602	GFP
SCD	1.30E-02	-1.492	1.54E-02	-1.520	GFP

*GO annotations[37,38].

Supplemental Figure 1

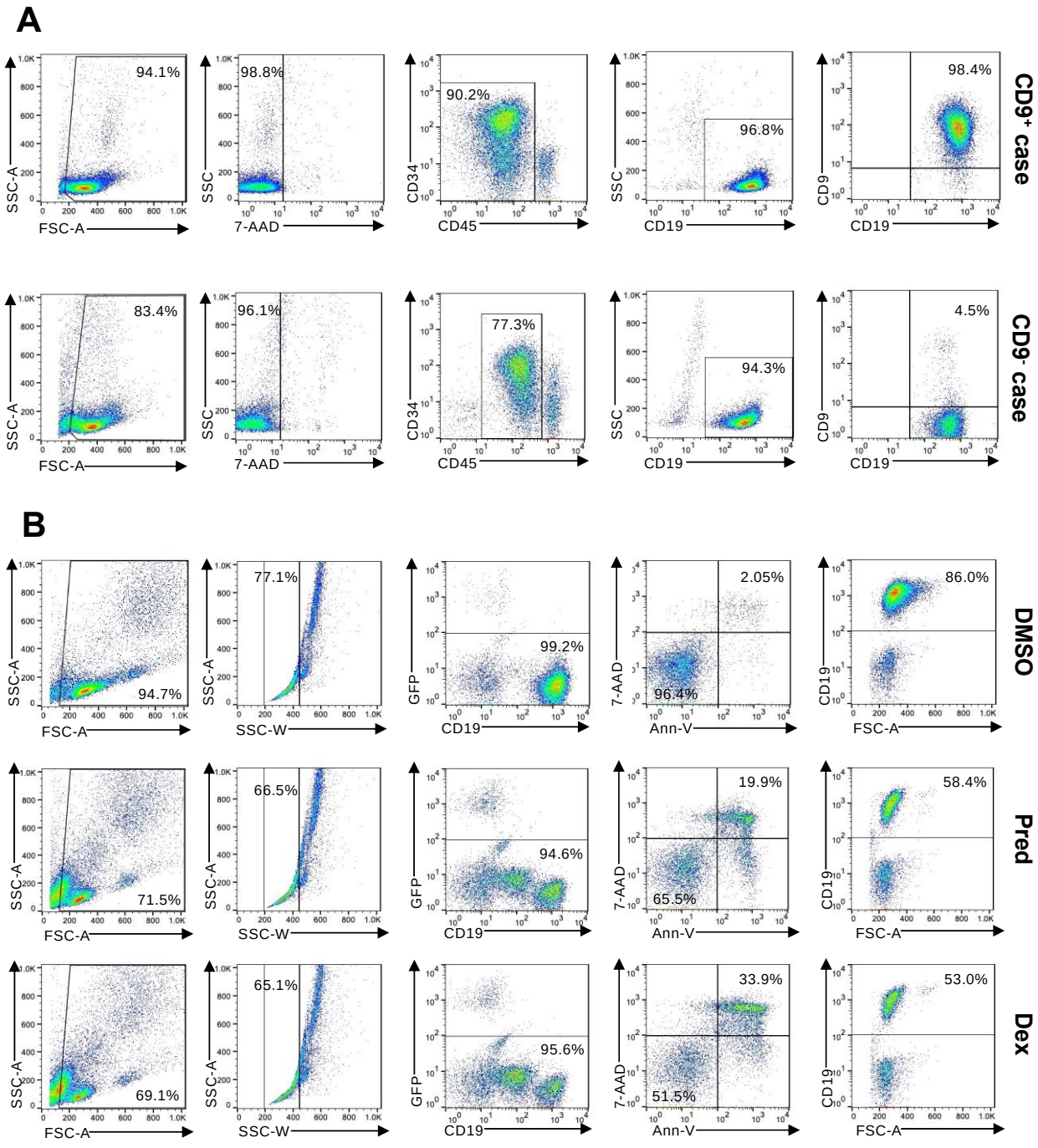

Supplemental Figure 1. Gating strategy for determination of CD9 expression and apoptosis in pediatric BCP-ALL samples. (A) Lymphoblasts were identified by light scattering properties with 7-AAD$^+$ cells excluded for analyses. CD45$^{dim/-}$CD34$^{+/-}$CD19$^+$ leukemic blasts were analyzed for CD9 expression with reference to the isotype controls. The sequential gating strategies of a CD9$^+$ (upper) and a CD9$^-$ (lower) case are shown. Positivity was defined by the presence of ≥20% CD9$^+$ blasts. (B)

Leukemic blasts in hTERT-MSC cocultures were identified by light scattering properties, followed by singlet selection by SSC parameters. GFP^- lymphoblasts were distinguished from GFP^+ MSCs and quantified for viable cells with Annexin $V^-/7\text{-}AAD^-$ phenotype. Viable lymphoblasts were further validated for CD19 expression. Shown are representative flow cytometry plots of a BCP-ALL sample treated with DMSO control, Dex (0.1 μM) or Pred (10 μM). Abbreviations: 7-AAD, 7-actino-aminomycin D; FSC, forward scatter; SSC, side scatter.

Supplemental Figure 2

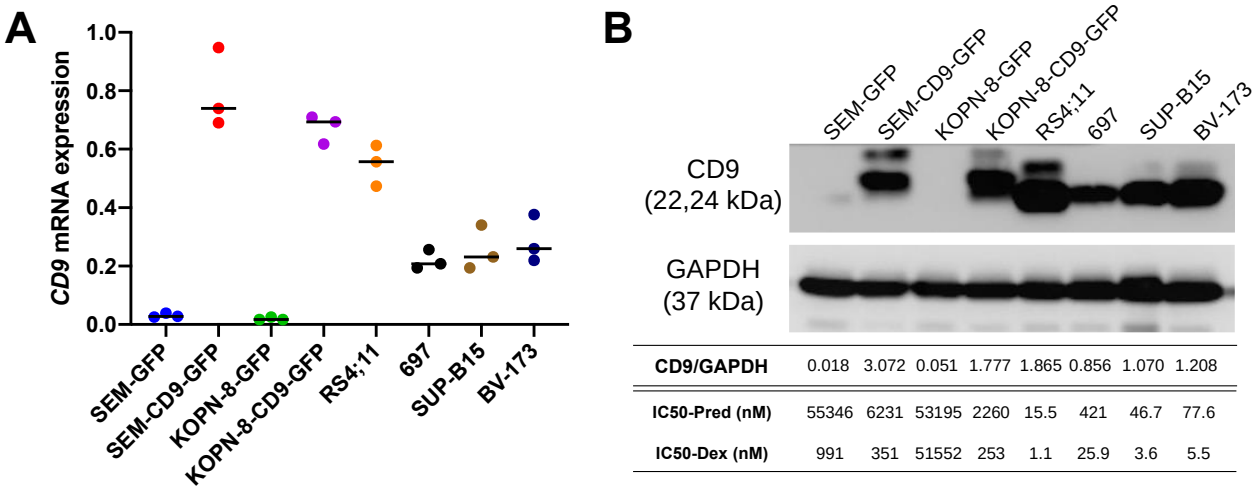

CD9/GAPDH	0.018	3.072	0.051	1.777	1.865	0.856	1.070	1.208
IC50-Pred (nM)	55346	6231	53195	2260	15.5	421	46.7	77.6
IC50-Dex (nM)	991	351	51552	253	1.1	25.9	3.6	5.5

Supplemental Figure 2. Comparison of CD9 expression and GC sensitivity among CD9-overexpressing and inherently CD9^{high} BCP-ALL cells. (A) *CD9* mRNA levels in CD9-transduced versus CD9^{high} BCP-ALL cells as determined by qRT-PCR (n=3). Expression was normalized to *GAPDH*. (B) CD9 protein levels in CD9-transduced versus CD9^{high} BCP-ALL cells as determined by Western blotting. Shown are representative images of 2 independent measurements. CD9/GAPDH ratio and Pred/Dex IC50s are indicated.

Supplemental Figure 3

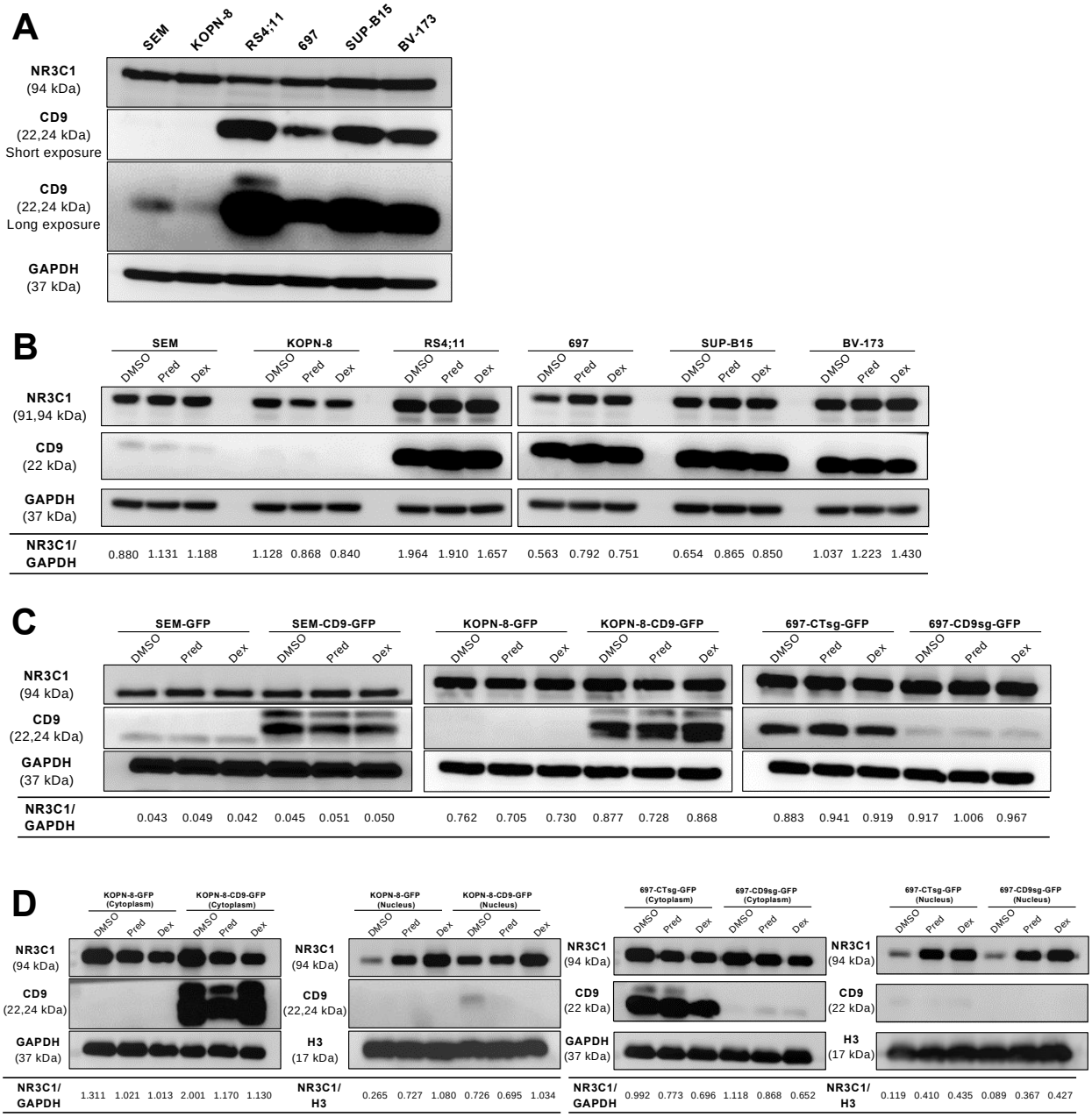

Supplemental Figure 3. CD9 does not affect the expression or nuclear translocation of NR3C1. (A) Expression of total NR3C1 in (A) $CD9^{high}$ (n=4) or $CD9^{low}$ (n=2) BCP-ALL cell lines as revealed by Western blotting, with GAPDH as the internal control. (B) Parental BCP-ALL cell lines were treated with respective IC50 concentrations of Pred (SEM, 30 μM; KOPN-8, 15 μM; RS4;11, 0.02 μM; 697, 0.5 μM; SUP-B15, 0.05 μM; BV-173, 0.1 μM) or Dex (SEM, 0.5 μM; KOPN-8, 1 μM; RS4;11, 0.001 μM; 697, 0.03 μM; SUP-B15, 0.005 μM; BV-173, 0.005 μM) for 8 hours. (C,D) Transduced BCP-ALL cell lines were treated with respective IC50 concentrations of Pred (SEM, 50 μM; KOPN-8, 50

μM; 697; 0.3 μM) or Dex (SEM, 1 μM; KOPN-8, 50 μM; 697, 0.02 μM) for 8 hours. The expression level of NR3C1 in (B,C) whole cell lysates or (D) fractionated cell lysates was measured by Western blotting. NR3C1/GAPDH or NR3C1/H3 intensity ratios are indicated.

Supplemental Figure 4

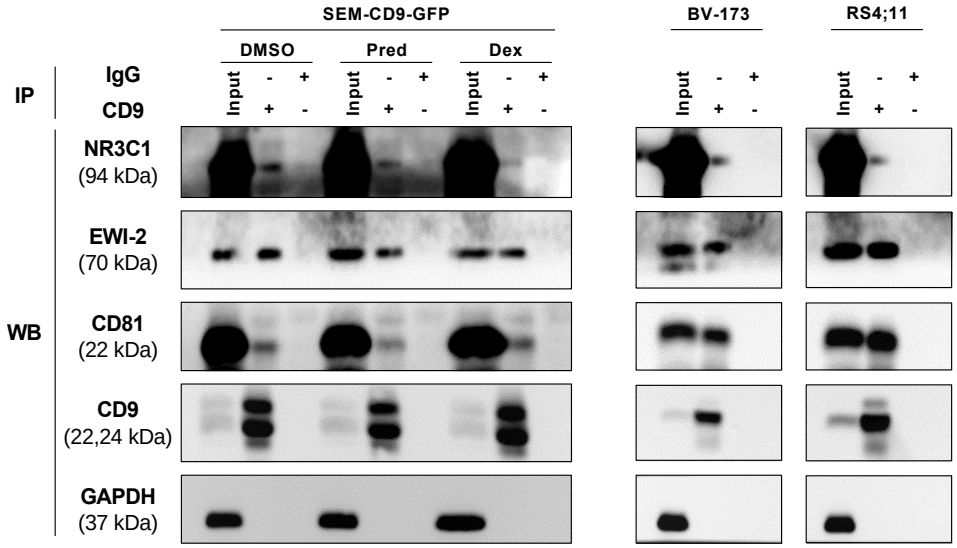

Supplemental Figure 4. NR3C1 physically interacts with CD9 in the tetraspanin-enriched microdomain. Transduced SEM-CD9-GFP as well as inherently $CD9^{high}$ BV-173 and RS4;11 BCP-ALL cells were treated with DMSO, Pred (50μM) or Dex (1μM) for 8 hours. Lysates were immunoprecipitated with IgG_{2b} or anti-CD9, and probed with antibodies against NR3C1 and the well-known TEM components EWI-2 and CD81. The presented images are representative of 3 independent experiments.

Supplemental Figure 5

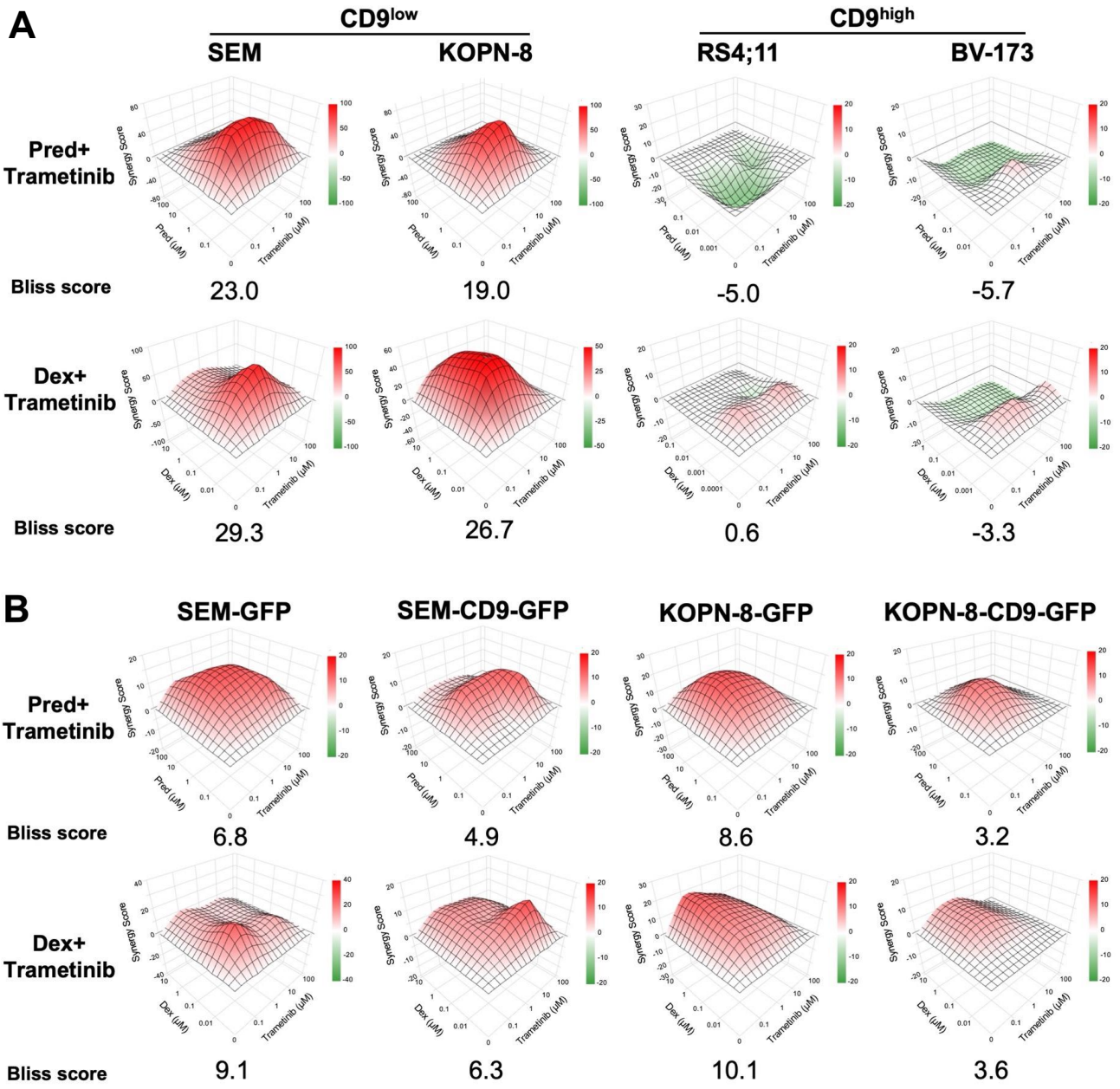

Supplemental Figure 5. MEK inhibitor synergistically increases the vulnerability of CD9^{low} BCP-ALL cells to GCs. (A) CD9^{low} (SEM, KOPN-8) and CD9^{high} (RS4;11, BV-173) BCP-ALL cells as well as (B) CD9-transduced cells were treated with combinations of trametinib (0.1 μM-100 μM) and Pred (1 nM-100 μM) or Dex (0.1 nM-10 μM) for 72 hours. For parental cells, the dose ranges of GCs were determined by their respective IC50s to ensure optimal model fitting. Drug interactions were calculated by the Bliss independence model, with relative cell viability normalized to DMSO controls as the experimental variable. The synergy map simulates the mode of drug interaction, with the color

bar indicating the excess over Bliss score at individual combinations. The overall mean Bliss scores of the combinations are indicated at the bottom: >0, overall synergy; =0, independence; <0, overall antagonism.

Supplemental Figure 6

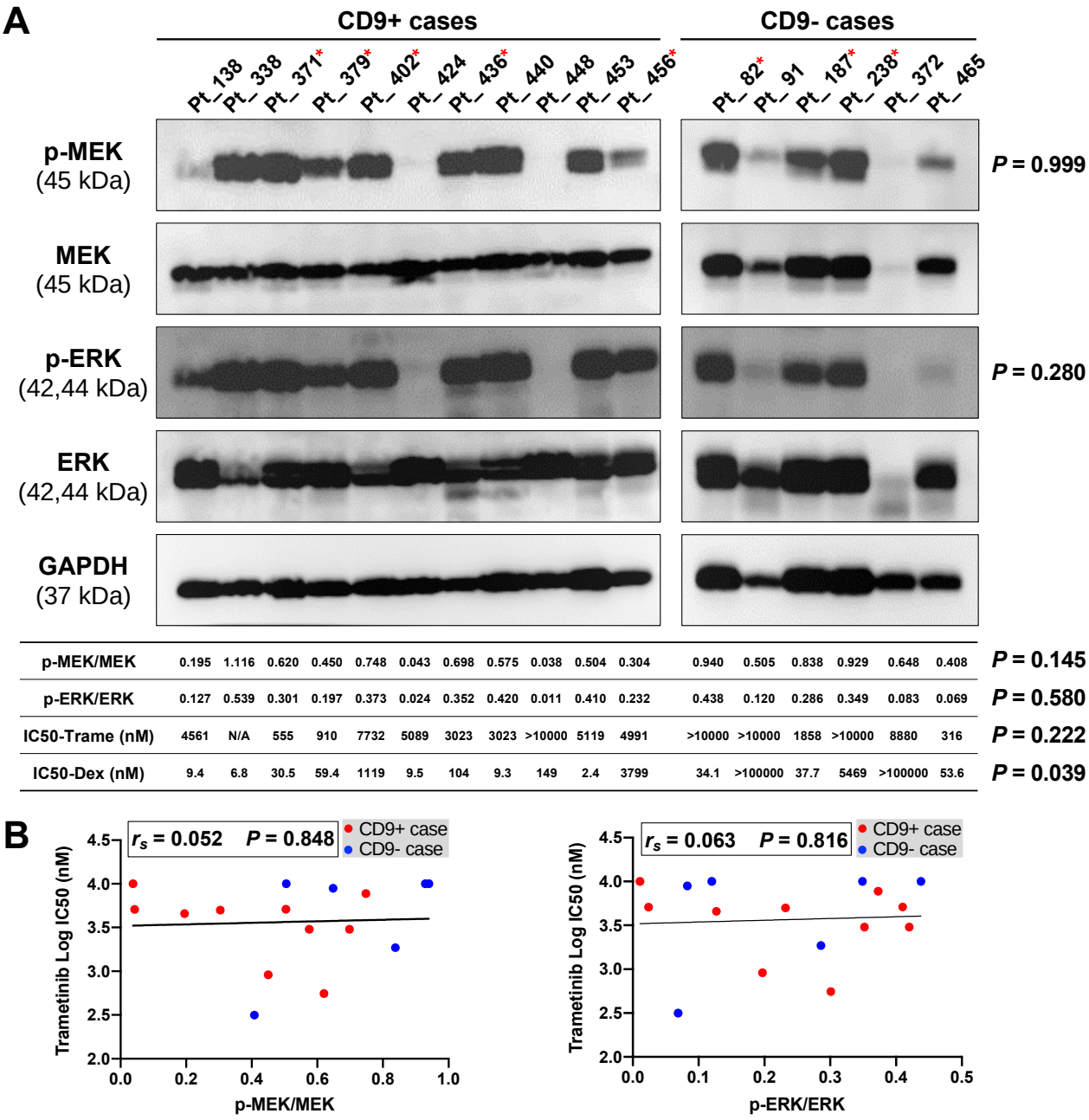

Supplemental Figure 6. Sensitivity of BCP-ALL cells to trametinib could not be predicted by activation status of MEK or ERK. (A) Basal expression level of key MAPK pathway components in BCP-ALL samples ($CD9^+$, n=11; $CD9^-$, n=6) as measured by Western blotting. Annotated are the normalized levels of p-MEK and p-ERK as well as the IC50s of trametinib and Dex of each sample. Asterisks denote samples chosen for drug combination experiments. (B) Correlation of MEK/ERK activation status with trametinib sensitivity. Statistics: (A) Fisher's exact test for comparing the p-MEK and p-ERK status between $CD9^+$ and $CD9^-$ cases; two-tailed, unpaired Student's *t*-test for

comparing the p-MEK/MEK and p-ERK/ERK ratio as well as trametinib and Dex sensitivity between $CD9^+$ and $CD9^-$ cases; (B) Spearman's correlation for determining the association of MEK and ERK activation with trametinib sensitivity.

Supplemental References

1. Lee SHR, Yang W, Gocho Y, et al. Pharmacotypes across the genomic landscape of pediatric acute lymphoblastic leukemia and impact on treatment response. Nat Med. 2023;29(1):170–179.
2. Wang H, Chan KYY, Cheng CK, et al. Pharmacogenomic profiling of pediatric acute myeloid leukemia to identify therapeutic vulnerabilities and inform functional precision medicine. Blood Cancer Discov. 2022;3(6):516–535.
3. Zhou Q, Yang J-J, Chen Z-H, et al. Serial cfDNA assessment of response and resistance to EGFR-TKI for patients with EGFR-L858R mutant lung cancer from a prospective clinical trial. J Hematol Oncol. 2016;9(1):86.
4. Ianevski A, Giri AK, Aittokallio T. SynergyFinder 2.0: visual analytics of multi-drug combination synergies. Nucleic Acids Res. 2020;48(W1):W488–W493.
5. Li CK, Chik KW, Ha SY, et al. Improved outcome of acute lymphoblastic leukaemia treated by delayed intensification in Hong Kong children: HKALL97 study. Hong Kong Med J. 2006;12(1):33–39.
6. Stary J, Zimmermann M, Campbell M, et al. Intensive chemotherapy for childhood acute lymphoblastic leukemia: Results of the randomized intercontinental trial ALL IC-BFM 2002. J Clin Oncol. 2014;32(3):174–184.
7. Cui L, Li ZG, Chai YH, et al. Outcome of children with newly diagnosed acute lymphoblastic leukemia treated with CCLG-ALL 2008: The first nation-wide prospective multicenter study in China. Am J Hematol. 2018;93(7):913–920.
8. Chan KYY, Zhang C, Wong YTS, et al. R4 RGS proteins suppress engraftment of human hematopoietic stem/progenitor cells by modulating SDF-1/CXCR4 signaling. Blood Adv. 2021;5(21):4380–4392.
9. Dobin A, Davis CA, Schlesinger F, et al. STAR: ultrafast universal RNA-seq aligner. Bioinformatics. 2013;29(1):15–21.
10. Zhang C, Zhang B, Lin L-L, Zhao S. Evaluation and comparison of computational tools for RNA-seq isoform quantification. BMC Genomics. 2017;18(1):583.
11. Liu T, Rao J, Hu W, et al. Distinct genomic landscape of Chinese pediatric acute myeloid leukemia impacts clinical risk classification. Nat Commun. 2022;13(1):1640.
12. Li H, Durbin R. Fast and accurate short read alignment with Burrows-Wheeler transform. Bioinformatics. 2009;25(14):1754–1760.
13. Zhang Y, Liu T, Meyer CA, et al. Model-based analysis of ChIP-Seq (MACS). Genome Biol. 2008;9(9):R137.
14. Wang Q, Li M, Wu T, et al. Exploring Epigenomic Datasets by ChIPseeker. Curr Protoc. 2022;2(10):e585.
15. Yu G, Wang L-G, He Q-Y. ChIPseeker: an R/Bioconductor package for ChIP peak annotation, comparison and visualization. Bioinformatics. 2015;31(14):2382–2383.
16. Kerstjens M, Pinhancos SS, Castro PG, et al. Trametinib inhibits RAS-mutant MLL-rearranged acute lymphoblastic leukemia at specific niche sites and reduces ERK phosphorylation in vivo. Haematologica. 2018;103(4):e147–e150.
17. Mir BA, Islam R, Kalanon M, Russell AP, Foletta VC. MicroRNA suppression of stress-responsive NDRG2 during dexamethasone treatment in skeletal muscle cells. BMC Mol Cell Biol. 2019;20(1):12.
18. Tissing WJE, den Boer ML, Meijerink JPP, et al. Genomewide identification of prednisolone-responsive genes in acute lymphoblastic leukemia cells. Blood. 2007;109(9):3929–3935.
19. Webb MS, Miller AL, Thompson EB. In CEM cells the autosomal deafness gene dfna5 is regulated by glucocorticoids and forskolin. J Steroid Biochem Mol Biol. 2007;107(1–2):15–21.
20. Nold V, Richter N, Hengerer B, Kolassa IT, Allers KA. FKBP5 polymorphisms induce differential

glucocorticoid responsiveness in primary CNS cells – First insights from novel humanized mice. Eur J Neurosci. 2021; 53(2):402-415.
21. Wolff NC, McKay RM, Brugarolas J. REDD1/DDIT4-independent mTORC1 inhibition and apoptosis by glucocorticoids in thymocytes. Mol Cancer Res. 2014;12(6):867–877.
22. Shi C, Huang P, Kang H, et al. Glucocorticoid inhibits cell proliferation in differentiating osteoblasts by microRNA-199a targeting of WNT signaling. J Mol Endocrinol. 2015;54(3):325–337.
23. Hong SG, Sato N, Legrand F, et al. Glucocorticoid-induced eosinopenia results from CXCR4-dependent bone marrow migration. Blood. 2020;136(23):2667–2678.
24. Choi GE, Chae CW, Park MR, et al. Prenatal glucocorticoid exposure selectively impairs neuroligin 1-dependent neurogenesis by suppressing astrocytic FGF2-neuronal FGFR1 axis. Cell Mol Life Sci. 2022;79(6):294.
25. Chen N, Meng Y, Zhan H, Li G. Identification and Validation of Potential Ferroptosis-Related Genes in Glucocorticoid-Induced Osteonecrosis of the Femoral Head. Medicina (Kaunas). 2023;59(2):297.
26. Zhang Q, Sun C, Liu X, Zhu C, Ma C, Feng R. Mechanism of immune infiltration in synovial tissue of osteoarthritis: a gene expression-based study. J Orthop Surg. 2023;18(1):58.
27. Sharma A, Menche J, Huang CC, et al. A disease module in the interactome explains disease heterogeneity, drug response and captures novel pathways and genes in asthma. Hum Mol Genet. 2015;24(11):3005–3020.
28. Yurtsever T, Streit F, Foo JC, et al. Temporal dynamics of cortisol-associated changes in mRNA expression of glucocorticoid responsive genes FKBP5, GILZ, SDPR, PER1, PER2 and PER3 in healthy humans. Psychoneuroendocrinology. 2019;10263–10267.
29. Wang X, Li Q, Li W, et al. Dexamethasone attenuated thoracic aortic aneurysm and dissection in vascular smooth muscle cell Tgfbr2-disrupted mice with CCL8 suppression. Exp Physiol. 2022;107(6):631–645.
30. Scheijen B, Boer JM, Marke R, et al. Tumor suppressors BTG1 and IKZF1 cooperate during mouse leukemia development and increase relapse risk in B-cell precursor acute lymphoblastic leukemia patients. Haematologica.2017;102(3):541-551.
31. Saenz GJ, Hovanessian R, Gisis AD, Medh RD. Glucocorticoid-mediated co-regulation of RCAN1-1, E4BP4 and BIM in human leukemia cells susceptible to apoptosis. Biochem Biophys Res Commun. 2015;463(4):1291–1296.
32. Cruz-Topete D, He B, Xu X, Cidlowski JA. Krüppel-like Factor 13 Is a Major Mediator of Glucocorticoid Receptor Signaling in Cardiomyocytes and Protects These Cells from DNA Damage and Death. J Biol Chem. 2016;291(37):19374–19386.
33. Jiang D, Jin H, Zuo J, et al. Potential biomarkers screening to predict side effects of dexamethasone in different cancers. Mol Genet Genomic Med. 2020;8(4):e1160.
34. Koide H, Holmbeck K, Lui JC, et al. Mice Deficient in AKAP13 (BRX) Are Osteoporotic and Have Impaired Osteogenesis. J Bone Miner Res. 2015;30(10):1887–1895.
35. Dong H, Zitt C, Auriga C, Hatzelmann A, Epstein PM. Inhibition of PDE3, PDE4 and PDE7 potentiates glucocorticoid-induced apoptosis and overcomes glucocorticoid resistance in CEM T leukemic cells. Biochem Pharmacol. 2010;79(3):321–329.
36. Chen DW-C, Lynch JT, Demonacos C, Krstic-Demonacos M, Schwartz J-M. Quantitative analysis and modeling of glucocorticoid-controlled gene expression. Pharmacogenomics. 2010;11(11):1545–1560.
37. Ashburner M, Ball CA, Blake JA, et al. Gene Ontology: tool for the unification of biology. Nat Genet. 2000;25(1):25–29.
38. Aleksander SA, Balhoff J, Carbon S, et al. The Gene Ontology knowledge base in 2023. Genetics. 2023;224(1):iyad031.